Journal of Materials Science: Materials in Medicine (2020) 31:29
https://doi.org/10.1007/s10856-020-06368-8

ENGINEERING AND NANO-ENGINEERING APPROACHES FOR MEDICAL DEVICES

Original Research

Effect of nanoscale bioactive glass with radial spherical particles on osteogenic differentiation of rat bone marrow mesenchymal stem cells

Lili Wang[1] · Jia Yan[1] · Xiaokun Hu[1] · Xinchen Zhu[1] · Shuying Hu[1] · Jun Qian[1] · Feimin Zhang[1] · Mei Liu[1]

Received: 26 August 2019 / Accepted: 20 February 2020 / Published online: 5 March 2020

Abstract

To validate the feasibility of two types of bioactive glass that contains spherical and radical spherical nano-sized particles in promoting bone repair, we hypothesize that radical spherical nano-sized particles have higher bone repair effectiveness than spherical one due to the physicochemical properties. We rigorously compared the physicochemical properties and bioactivities of these two types of bioactive glass. Specifically, we measured the size, surface morphology, concentration of ionic-dissolution products, bioactivity, and biological effects of two groups of bioactive glass on rat bone marrow mesenchymal stem cells (rBMSCs) and evaluate their effect on proliferation and osteogenic differentiation of rBMSCs in vitro. We observed that spherical nano-bioactive glass (SNBG) was spherical with smooth boundary, while the radial spherical nano-bioactive glass (RSNBG) had radial pore on the surface of particle boundary. When the two materials were immersed in simulated body fluid for 24 h, RSNBG produced more and denser hydroxyapatite carbonate than SNBG. The concentration of Ca and Si ions in RSNBG 24 h extract is higher than that of SNBG, while the concentration of P ions is lower. Proliferation, alkaline phosphatase (ALP) activity, intracellular Ca ion concentrations defined as the number of mineralized nodules produced, and the expression of osteogenic genes were significantly higher in rBMSCs co-cultured with 50 μg/mL RSNBG than SNBG. Overall, these results validated our hypothesis that RSNBG can provide better benefit than SNBG for inducing proliferation and osteogenic differentiation in rBMSCs, in turn suggested the feasibility of this RSNBG in further studies and utilization toward the ends of improved bone repair effectiveness.

Graphical Abstract

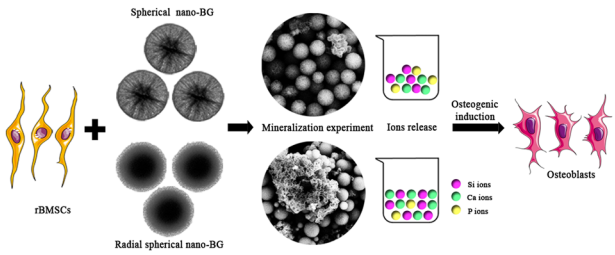

1 Introduction

Effective repair and reconstruction of craniomaxillofacial bone defects caused by tumor, trauma, or periodontal disease is a major challenge in maxillofacial surgery and dentistry [1]. Autografts, allografts, and biomaterials have been most commonly used to repair and reconstruct these bone defects [2, 3]. However, due to limited supply and

✉ Feimin Zhang
fmzhang@njmu.edu.cn

✉ Mei Liu
liumei2017@njmu.edu.cn

[1] Jiangsu Key Laboratory of Oral Diseases, Department of Prosthodontics, Affiliated Hospital of Stomatology, Nanjing Medical University, Nanjing 210029 Jiangsu, China

plastic restriction, autologous bone grafts drew significant concern for repair bulk bone defects.

Because of the risk of tissue rejection and disease transmission, the clinical applications of allografts are also remarkably limited. In this case, research has begun to focus on the use of biomaterials as a surrogate approach in orthopedic repair procedures. As a result, various types of biomaterials have been developed that have potential being utilized in bone defects repair, such as ceramics, polymers, composite materials, etc [4]. Particularly, bioactive glass, which is a type of bioceramics, has become a promising bone graft material because of its good biocompatibility, bone conduction, and bone induction [5, 6]. In the late 1960s, Hench produced the first generation of bioactive glass, Bioglass 45S5, composed of 46.1 mol% SiO_2, 22.4 mol% Na_2O, 26.9 mol% CaO, and 2.6 mol% P_2O_5 [7], which binds firmly to bone tissue [8]. In 1985, bioactive glass was clinically applied in orthopedics and stomatology. The success in both manufacturing and clinical application encouraging extensive studies on bioactive glass [9], aims to further understand the mechanism behind its capability in facilitating bone defect repair as well as optimize the design for higher defect repair effectiveness.

Of note, when inserted into a bone defect, bioactive glass has the unique ability to bond host bone and stimulate the growth of new bone [10, 11]. Underlying mechanisms of bone growth include the induction of biological reactions at the interface of the bioactive glass and bone-forming cells and within those cells, to promote proliferation and differentiation [12, 13]. Concomitantly, bioactive glass is a degradable material. Ionic-dissolution products released from the bioactive glass create a local environment conducive to cell aggregation, proliferation, and differentiation, and can promote the expression of osteoblasts-related genes [12, 13]. When bioactive glass is exposed to biological fluid, there is an initial dissolution stage followed by the formation of a hydroxyl carbonate apatite (HCA) layer on its surface [8]. The HCA layer is similar to the mineral phase in bone and can bond to collagen fibers [14, 15].

However, several limitations still need to be addressed before bioactive glass being widely utilized in clinical practice. Most notably, the bone repair effectiveness still needs further improvement, which can at least partly attribute to the size and morphologies of the glass particles [15]. Studies have demonstrated the bioactive glass with nano-sized particles exhibits better biological performance than bioactive glass with micron-sized particles that are currently used [16], and the mechanism behind which can be attributed to the much larger specific surface area possessed by nanoscale bioactive glass than traditional bioactive glass [17]. On the one hand, the large specific surface area provides more surface adsorption sites, rendering the nano-bioactive glass higher biological activity than the conventional ones [18, 19]. On the other hand, the large specific surface area facilitates the degradation of nanoscale bioactive glass [20], and the Ca, Si, and P ions released resulted from the degradation in turn promote the formation of HCA and tissue bonding [21, 22].

Compared with irregularly shaped particles, bioactive glass with spherical particles exhibits superior biological activity and increased osteogenic potential due to regular shape and better flow property [23]. Wang et al. demonstrated that the spherical bioactive glass (molar composition: 58% SiO_2, 33% CaO, 9% P_2O_5) can strongly promote the osteoblast differentiation [24]. Build on this foundation, we hypothesize that further increase in the surface area could improve osteogenic potential of bioactive glass. Aiming to proof of this concept, we incorporate "radial" spherical particles into bioactive glass, which has proven having higher specific surface area than spherical particles by Li et al [25]. The physical and chemical properties of two novel spherical and radioactive globular nano-bioactive glasses provided by Chen et al. were characterized, the effects of the two materials on the proliferation and osteogenic differentiation of rat bone marrow mesenchymal stem cells (rBMSCs) were evaluated to explore the feasibility and advantages of using them as bone biomaterials for repairing bone defects.

2 Materials and methods

2.1 Synthesis of bioactive glass

Bioactive glass was kindly provided by the Xiaofeng Chen project group of the South China University of Technology. Spherical nano-bioactive glass (SNBG) (90 mol% SiO_2, 6 mol % CaO, and 4 mol% P_2O_5) and radial spherical nano-bioactive glass (RSNBG) (60 mol% SiO_2, 36 mol% CaO, and 4 mol% P_2O_5) were prepared using the sol–gel method [26].

2.2 Characterization of bioactive glass

2.2.1 Size of bioactive glass particles

The size of the bioactive glass particles was measured using a Laser particle size analyzer (NANO-ZS, Malvern, Worcestershire, UK).

2.2.2 Morphology of bioactive glass particles

The surface morphology of the bioactive glass was observed using a scanning electron microscope (SEM, Ultra Plus, Zeiss, Jena, Germany) and a transmission electron microscope (TEM, JEM-200CX, JEOL, Tokyo, Japan).

2.2.3 Bioactive glass extraction

Bioactive glass extracts were prepared by incubating bioactive glass in 1 mg/mL α-Minimum Essential Medium (α-MEM, Gibco, Gaithersburg, USA) on a thermostatic shaker (150 rpm/h) at 37 °C for 24 h. Samples were centrifuged and the supernatant was filtered using a 0.22 μm pore size filter (Millipore, Billerica, USA). Extracts were evaluated with inductively coupled plasma-optical emission spectroscopy (ICP-OES, iCAP 7400, Thermo, Waltham, USA) to determine Si, Ca, and P ion concentrations.

2.2.4 Bioactivity of bioactive glass in vitro

The bioactivity (bonding-bone ability) of the bioactive glass was indirectly evaluated in vitro by determining the ability of the glass to induce HCA formation on its surface [26]. Bioactive glass was incubated in 1 mg/mL simulated body fluid (SBF, pH 7.4), which has the same composition as human plasma. The mixtures were placed on a thermostatic shaker (150 rpm/h) at 37 °C for 24 h, centrifuged, and then the precipitate was collected, washed three times with acetone and distilled water, and placed at 65 °C for 48 h to dry. Newly formed HCA on the bioactive glass surface was observed by SEM and Fourier Transform Infrared spectroscopy (FTIR, SpectrumGX, PerkinElmer, Waltham, USA).

2.3 Biological effects of bioactive glass on rBMSCs in vitro

2.3.1 Cell culture

OriCell Sprague-Dawley (SD) rBMSCs (Passage [P] 2), OriCell SD rBMSCs growth medium, and OriCell SD rBMSCs osteogenic differentiation medium were purchased from Cyagen Biosciences (Guangzhou, China). rBMSCs were cultured in a 5% CO_2 incubator at 37 °C. Adherent cells were passaged at approximately 80% confluence. P 3–5 cells were used in subsequent experiments. Culture medium was changed every 2–3 days.

For cell proliferation assays, rBMSCs were seeded at 2×10^3 cells/well in a 96-well plate and cultured in OriCell SD rBMSCs growth medium. For cell cycle analysis, rBMSCs were seeded at 2×10^4 cells/well in a 24-well plate and cultured in OriCell SD rBMSCs growth medium. After the cells were attached, 30, 50, 80, and 100 μg/mL bioactive glass was added to the growth medium.

For osteogenic differentiation analyses, rBMSCs were seeded at 2×10^4 cells/well in OriCell SD rBMSCs osteogenic differentiation medium in 24-well plates. After the cells were attached, 50 μg/mL bioactive glass was added to the osteogenic differentiation medium. Cells were incubated with bioactive glass for up to 21 days, depending on the assay. Culture medium without bioactive glass was used as a blank control.

2.3.2 Cell proliferation assay

rBMSCs proliferation was determined using the Cell Counting Kit-8 (CCK-8, Beyotime, Shanghai, China). rBMSCs were incubated with bioactive glass for 7 days. On days 0, 1, 3, 5, and 7 of culture the number of rBMSCs was detected using the CCK-8 according to the manufacturer's instructions. Briefly, the original culture medium was discarded, and 100 μL of fresh complete medium containing 10% kit medium was added to each well. After incubation in the dark at 37 °C for 2 h, the medium was aspirated and absorbance was measured at 450 nm using a microplate reader (Spectra Max190, Molecular Device LLC, Sunnyvale, USA).

2.3.3 Cell cycle analysis

Cell cycle analysis was conducted using flow cytometry. rBMSCs were incubated with bioactive glass for 7 days. On days 3 and 7 of culture the cells were digested, precipitated by centrifugation, washed twice with phosphate-buffered saline (PBS), and fixed in 75% ethanol at 4 °C for 24 h. Samples were centrifuged to obtain a precipitate, which was washed three times with PBS. 100 mL 10% propidium iodide (Sigma, St.Louis, USA) was added and samples were incubated on ice for ~30 min. Flow cytometry (FACSCalibur, Becton Dickinson, San Jose, USA) and Cell Quest software were used to identify cells in various stages of the cell cycle.

2.3.4 Alkaline phosphatase (ALP) staining and activity assay

For ALP staining, rBMSCs were stained with the 5-bromo-4-chloro-3-indolyl phosphate/nitroblue tetrazolium chloride (BCIP/NBT) ALP Color Development Kit (Beyotime Biotechnology, Shanghai, China) according to the manufacturer's instructions. Briefly, rBMSCs were fixed with 4% paraformaldehyde for 30 min and washed with PBS three times. rBMSCs were stained with BCIP/NBT reagents and washed with distilled water three times before observation.

On days 5 and 7 of osteogenic induction, rBMSCs were lysed on ice with 0.5% Triton X-100 for 30 min, and supernatants were collected for determination of ALP activity and total cell protein content. The ALP Assay kit (Jiancheng Bioengineering Institute, Nanjing, China) and the BCA Protein Assay Kit (Leagene Biotechnology, Beijing, China) were used to determine ALP activity and total cell protein content, respectively. Both assays were performed according to the manufacturer's instructions. ALP activity was standardized to total cellular protein content.

2.3.5 Matrix mineralization

Matrix mineralization was assessed using alizarin red staining. rBMSCs were incubated with bioactive glass for 21 days. On days 14 and 21 of culture cells were fixed in 4% paraformaldehyde for 10 min and stained with 1% alizarin red staining (Leagene Biotechnology, Beijing, China) at 37 °C for 5 min. Microscopy was used to observe randomly selected fields of view ($n = 5$) and capture images of calcium nodules. Calcium deposits were semiquantified by the addition of 500 µL of 100 mM cetylpyridinium chloride (Sigma, St. Louis, USA) to each well at 37 °C for 30 min. Absorbance of the solution was measured at 562 nm using a microplate reader.

2.3.6 Real-time polymerase chain reaction (RT-PCR)

Expression of rBMSCs differentiation and mineralization markers was measured by RT-PCR. rBMSCs were incubated with bioactive glass for 14 days. On days 7 and 14 of culture total cellular RNA was extracted with a Trizol reagent (Invitrogen, Carlsbad, USA) and reverse transcribed (Promega, Madison, USA) to cDNA. RT-PCR was performed using a Faststart Universal SYBR Green PCR Master mix kit (Roche, Indianapolis, USA) and an ABI7300 thermocycler (Applied Biosystems Inc., Foster City, USA). The reaction conditions were: 95 °C for 30 s; 40 cycles of 95 °C for 10 s and 60 °C for 31 s; 95 °C for 15 s, 60 °C for 60 s, and 95 °C for 15 s. Primers were synthesized by Wuhan Google Biotechnology Co., Ltd. GAPDH was selected as an internal control. Primer sequences are shown in Table 1. The $2^{-\Delta\Delta Ct}$ method was used to calculate relative gene expression levels.

2.3.7 Western blot

Western Blot was performed to examine the protein levels of osteogenic markers (Runx2, COL1, and OSX). GAPDH was used as internal reference. On days 7 and 14 of osteogenic induction, rBMSCs were washed three times with the PBS and RIPA lysis buffer (EnoGene, Nanjing, China) and 1% phenylmethanesulfonyl fluoride (PMSF, EnoGene, Nanjing, China) was added. After ultrasonically shaken for 30 s, the supernatant was collected by centrifugation at 12000 rpm for 10 min. The total protein concentration of cells was determined using the BCA method. Sample buffer was added to the protein and boiled for 10 min before sodium dodecyl sulfate-polyacrylamide gel electrophoresis (SDS-PAGE) electrophoresis. Equal amounts of protein were loaded onto 10% SDS-PAGE gel and transferred onto a polyvinylidene difluoride membrane. The membrane was placed in Tris-buffered saline with 0.1% Tween-20 (TBST) (Biosharp, Hefei, China) containing 5% (w/v) skimmed milk powder (BBI Life Sciences Corporation, Shanghai, China) for 2 h. After incubating the membrane with diluted primary antibody (Abcam, Cambridge, UK) at 4 °C overnight, the membrane was washed three times with TBST and incubated in the diluted horseradish peroxidase-labeled secondary antibody (Abcam, Cambridge, UK) for 1 h at room temperature. After washing the membrane, the proteins were detected by chemiluminescence gel imaging system (Tanon 5200, Tanon, Shanghai, China). Western blot results were analyzed using the ImageJ (NIH, Bethesda, USA).

2.4 Statistical analysis

Quantitative data were expressed as mean ± standard deviation. Between-group differences were determined using one-way ANOVA. Statistical analysis was conducted using SPSS v.19.0 software (IBM Corporation, Armonk, USA). $P < 0.05$ was considered significant.

3 Results

3.1 Characterization of bioactive glass

3.1.1 Morphology and size distribution of bioactive glass particles

SEM and TEM micrographs demonstrated that the bioactive glass consists of nanoparticles with a regular spherical shape and good dispersibility both in SNBG (Fig. 1a, c) and RSNBG (Fig. 1b, d). Furthermore, the bioactive glass particles in RSNBG had fine branch-like structures on the surface. The particle size distribution was uniform in both SNBG and RSNBG. The average particle size of SNBG and RSNBG was 592.3 nm (Fig. 1a, inset) and 890.8 nm (Fig. 1b, inset), respectively.

Table 1 Primers for RT-PCR analysis

Gene	Forward primer (5′-3′)	Reverse primer (3′-5′)
Runx2	CCCAACTTCCTGTGCTCCGT	GCTCCGGCCTACAAATCTCAG
Col1	AGAGGCATAAAGGGTCATCGTG	AGACCGTTGAGTCCATCTTTGC
Osx	CTGGGAAAAGGAGGCACAAAGA	GGGGAAAGGGTGGGTAGTCATT
GAPDH	CTGGAGAAACCTGCCAAGTATG	GGTGGAAGAATGGGAGTTGCT

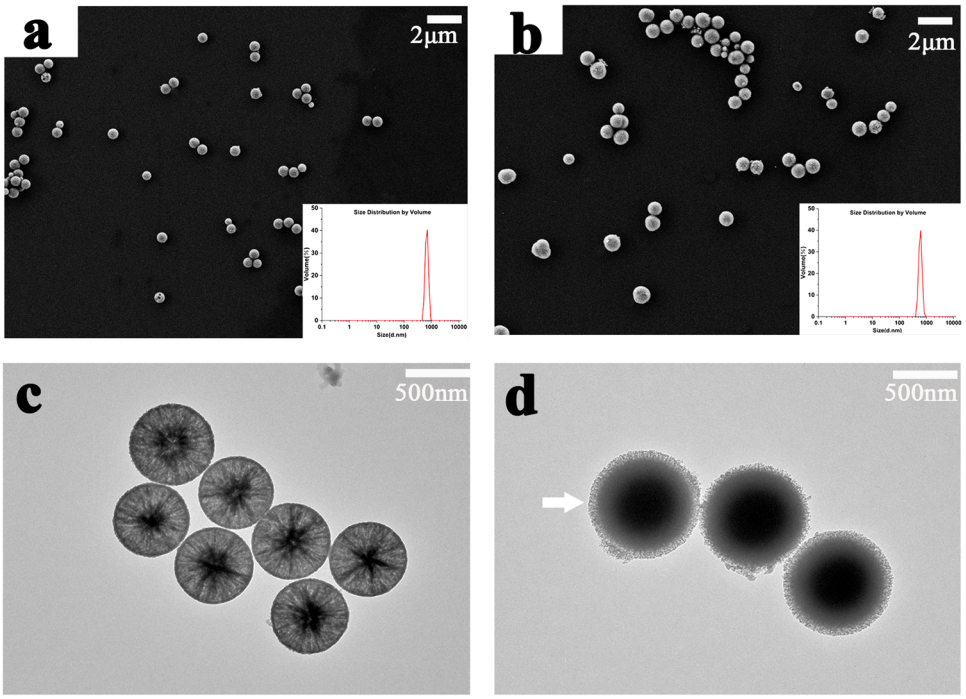

Fig. 1 Morphology and size distribution of bioactive glass particles. SEM images of the surface morphology of SNBG (**a**) and RSNBG (**b**). Particle size distribution of SNBG (**a**, inset) and RSNBG (**b**, inset). TEM images of the surface morphology of SNBG (**c**) and RSNBG (**d**) (arrow represents fine branch-like structures)

Table 2 Concentrations of Si, Ca, and P ions in the bioactive glass extracts

	Si (mg/L)	Ca (mg/L)	P (mg/L)
α-MEM	0.00 ± 0.00	73.24 ± 0.81	35.34 ± 0.60
SNBG	28.16 ± 0.40*	98.08 ± 0.54*	24.75 ± 0.28*
RSNBG	158.05 ± 1.90*,**	117.91 ± 0.62*,**	14.47 ± 0.75*,**

$n = 3$

*$P < 0.05$, versus blank control group; **$P < 0.05$, RSNBG versus SNBG

3.1.2 ICP-OES analysis

We further tested and compared the concentration of different ions in extracts of both SNBG and RSNBG, meanwhile quantitatively compared with cell culture medium (α-MEM). RSNBG extract contained a higher concentration of Si and Ca ions and a lower concentration of P ions compared with SNBG extract ($P < 0.05$) (Table 2). SNBG extract contained higher concentrations of Si and Ca ions than α-MEM but a lower concentration of P ions ($P < 0.05$).

3.1.3 Bioactivity of bioactive glass

The bioactivity of bone biomaterials can be indirectly evaluated by the ability to induce apatite formation on their surfaces in vitro [27]. After incubation in SBF for 24 h, the surface morphology of SNBG (Fig. 2a) and RSNBG (Fig. 2c) changed. A large number of compact plate-like deposits appeared on the surface of RSNBG, in contrast fewer deposits appeared on the surface of SNBG.

The FTIR spectra of SNBG and RSNBG (Fig. 2b, d) were similar before incubation in SBF, showing characteristic absorption bands of the following Si–O–Si bonds: 1060 cm^{-1} (asymmetric stretching vibration), 798 cm^{-1} (symmetric stretching vibration), and 480 cm^{-1} (bending vibration) [28]. New absorption bands attributed to bending vibrations of P–O (960 cm^{-1}) and C–O (875 cm^{-1}) bonds are in presence on the spectra of RSNBG but in absence on that of SNBG after incubation in SBF, indicating the formation of HCA on the surface of RSNBG but not SNBG. These data indicate that RSNBG has better bioactivity in vitro compared with SNBG after mineralizing for 24 h.

3.2 Biological effects of bioactive glass on rBMSCs in vitro

3.2.1 Cell proliferation assay and cell cycle analysis

To determine the optimal concentration of bioactive glass that facilitates the growth of rBMSCs, we incubated cells with different concentrations of SNBG or RSNBG, and found only 50 μg/mL SNBG or RSNBG significantly promoted the proliferation of rBMSCs within 7 days ($P < 0.05$) (Fig. 3a–c). Therefore, 50 μg/mL bioactive glass was used in subsequent experiments. In addition, proliferation of rBMSCs incubated with 50 μg/mL RSNBG was observed significantly greater compared with those incubated with

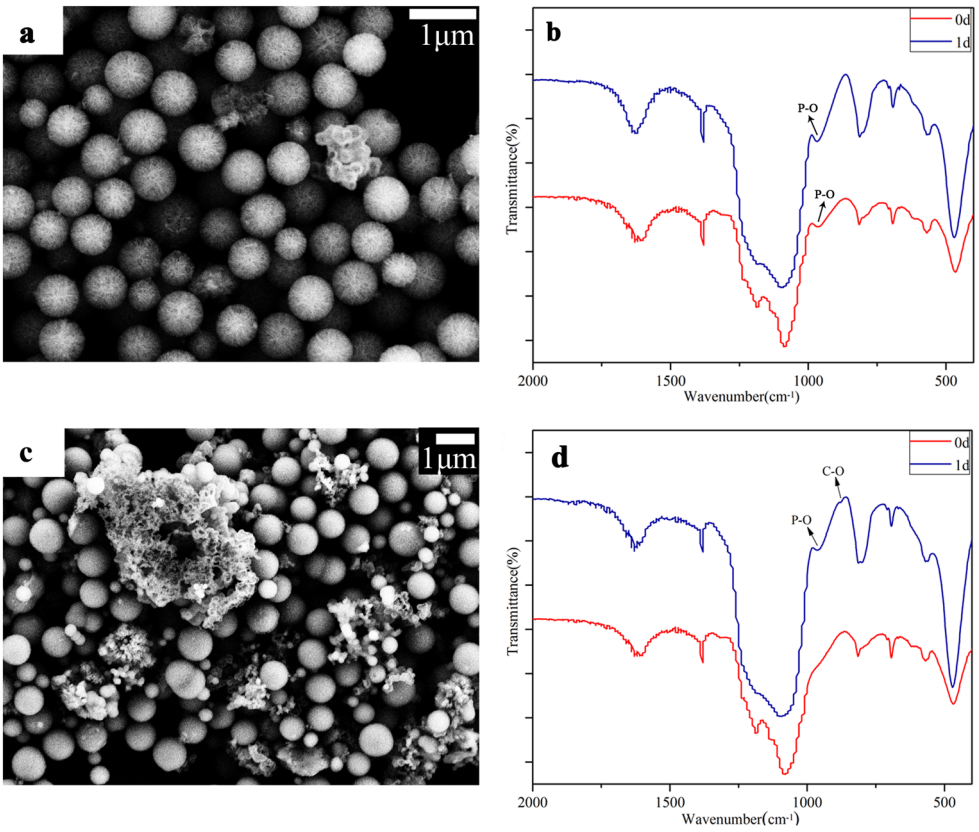

Fig. 2 Bioactivity of bioactive glass in vitro. SEM images of SNBG (**a**) and RSNBG (**c**) after incubating in SBF for 24 h. FTIR spectra of SNBG (**b**) and RSNBG (**d**) before and after incubating in SBF for 24 h

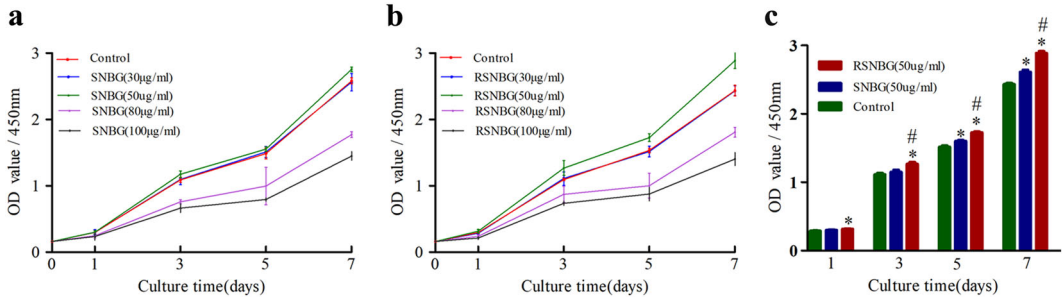

Fig. 3 CCK-8 analysis of rBMSCs proliferation. Growth curves of rBMSCs incubated with different concentrations of SNBG (**a**) and RSNBG (**b**) as determined by the CCK-8. **c** OD values of rBMSCs incubated with 50 μg/mL SNBG and 50 μg/mL RSNBG compared with untreated rBMSCs at days 1, 3, 5, and 7. Control, not incubated with bioactive glass; SNBG, incubated with SNBG; RSNBG, incubated with RSNBG. ($n = 3$; $^{*}P < 0.05$, versus blank control group; $^{\#}P < 0.05$, RSNBG versus SNBG)

50 μg/mL SNBG, which preliminarily validated the higher bioactivity of RSNBG over SNBG.

On days 3 and 7 of culture, the proliferation indices ($S\% + G_2/M\%$) of rBMSCs incubated with 50 μg/mL SNBG ($24.98 \pm 0.62\%$ at 3 days; $5.65 \pm 0.38\%$ at 7 days) or RSNBG ($28.18 \pm 1.37\%$ at 3 days; $6.52 \pm 0.39\%$ at 7 days) were significantly higher compared with the control group ($19.07 \pm 0.15\%$ at 3 days; $4.49 \pm 0.24\%$ at 7 days) ($P < 0.05$) (Fig. 4a, b). The proliferation index of rBMSCs incubated with RSNBG was significantly higher compared with the proliferation index of rBMSCs incubated with SNBG ($P < 0.05$). Flow cytometry analyses were consistent with findings from the CCK-8 assay. These data further validated that 50 μg/mL RSNBG is optimal for inducing rBMSCs proliferation.

3.2.2 ALP staining

On day 5 of culture, ALP activity was significantly increased in rBMSCs incubated with 50 μg/mL RSNBG compared with rBMSCs incubated with 50 μg/mL SNBG or the control group (Fig. 5). On day 7 of culture, no difference was found in ALP activity of rBMSCs incubated with RSNBG and SNBG, incubated both of which were significantly higher than the control group ($P < 0.05$).

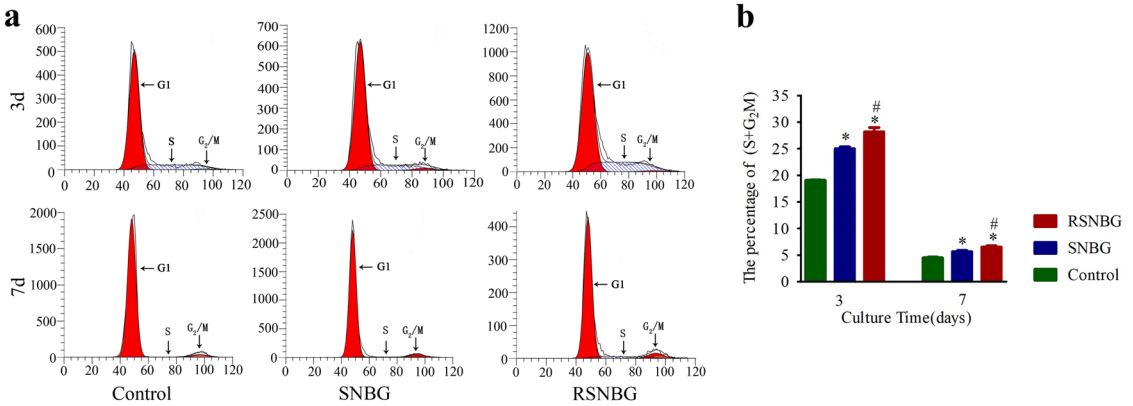

Fig. 4 Flow cytometry analysis of cell cycle distribution. Control, not incubated with bioactive glass; SNBG, incubated with SNBG; RSNBG, incubated with RSNBG. ($n = 3$; $^{*}P < 0.05$, versus blank control group; $^{\#}P < 0.05$, RSNBG versus SNBG)

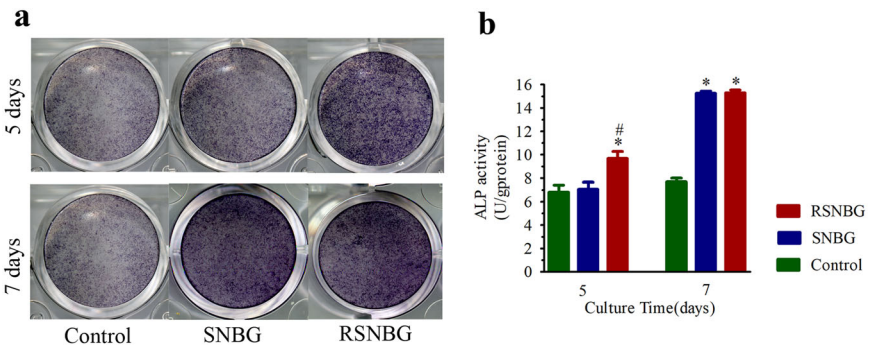

Fig. 5 Analysis of ALP staining and activity of rBMSCs. (**a**) ALP staining 5 and 7 days after osteogenic induction. (**b**) ALP activity 5 and 7 days after osteogenic induction. Control, not incubated with bioactive glass; SNBG, incubated with SNBG; RSNBG, incubated with RSNBG. ($n = 3$; $^{*}P < 0.05$, versus blank control group; $^{\#}P < 0.05$, RSNBG versus SNBG)

3.2.3 Matrix mineralization

On days 14 and 21 of culture, alizarin red staining revealed the presence of mineralized nodules in rBMSCs (Fig. 6a). Compared with the control group, the extracellular matrix of rBMSCs incubated with SNBG or RSNBG was more mineralized, and the higher density and larger area of red calcium nodule mass deposition were observed in the gross and microscopic images. The calcium nodule density in rBMSCs incubated with 50 μg/mL RSNBG was higher than SNBG.

Quasi-quantification of intracellular Ca ion concentrations demonstrated that rBMSCs incubated with both SNBG or RSNBG were significantly higher compared with the control group (Fig. 6b); incubated with RSNBG was also significantly higher than SNBG ($P < 0.05$). The trends were consistent in 14 and 21 days post incubation with both types of bioactive glass. In addition, the quasi-quantitative determination of calcium nodules content that in agreement with the results of alizarin red staining demonstrated the strong tendency of rBMSCs osteo-differentiation induced by both bioactive glass, especially the RSNBG.

3.2.4 RT-PCR

On days 7 and 14 of culture, osteogenic gene (Runx2, Col1, Osx) expression in rBMSCs incubated with 50 μg/mL RSNBG or SNBG was significantly higher compared with the control group ($P < 0.05$) (Fig. 7). Osteogenic gene expression was also higher in rBMSCs incubated with 50 μg/mL RSNBG compared with the rBMSCs incubated with 50 μg/mL SNBG ($P < 0.05$).

3.2.5 Western blot analysis

On days 7 and 14 of culture, the expression of relative proteins (Runx2, COL1, and OSX) presented the similar tendency with relative genes. The expression of relative proteins (Runx2, COL1, and OSX) in rBMSCs incubated with 50 μg/mL RSNBG or SNBG was significantly higher compared with the control group ($P < 0.05$) (Fig. 8). The expression of relative proteins (Runx2, COL1, and OSX) was also higher in rBMSCs incubated with 50 μg/mL RSNBG compared with the rBMSCs incubated with 50 μg/mL SNBG ($P < 0.05$).

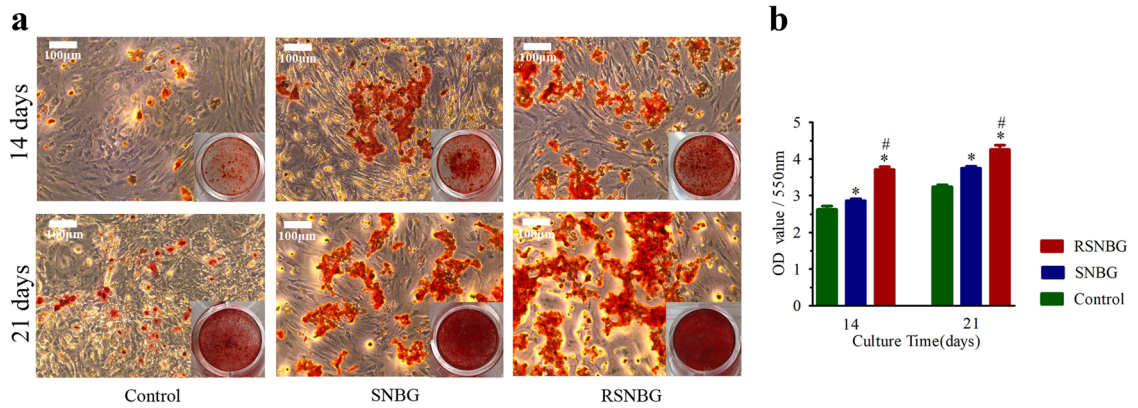

Fig. 6 Alizarin red staining and semi-quantitative analysis of calcium deposits. **a** Alizarin red staining of mineralized nodules after 14 and 21 days of osteogenic-inducing culture. **b** Semi-quantification of calcium deposits of rBMSCs incubated with and without bioactive glass. Control, not incubated with bioactive glass; SNBG, incubated with SNBG; RSNBG, incubated with RSNBG. ($n = 3$; $^{*}P < 0.05$, versus blank control group; $^{\#}P < 0.05$, RSNBG versus SNBG)

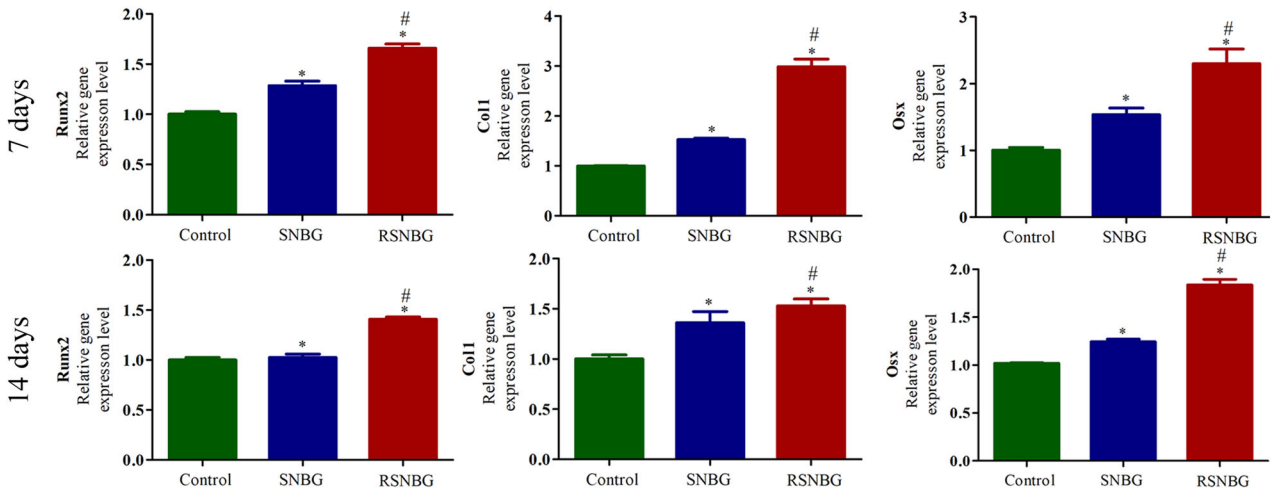

Fig. 7 RT-PCR analysis of osteogenic genes expression levels of rBMSCs at days 7 and 14 of culture. Control, not incubated with bioactive glass; SNBG, incubated with SNBG; RSNBG, incubated with RSNBG. ($n = 3$; $^{*}P < 0.05$, versus blank control group; $^{\#}P < 0.05$, RSNBG versus SNBG)

4 Discussion

As the third-generation biomaterials, bioactive glass owns strong bone conductivity and osteoinductivity [24], and therefore has been extensively applied clinically aiming for bone tissue repair and engineering [29]. In recent years, researches have demonstrated the merits of nano-bioactive glass, for example larger specific surface area, better bioactivity and more potent in guiding osteoblasts adhesion over traditional bioactive glass [30, 31]. Particularly, in the family of bioactive glass, the spherical bioactive glass has emerged as a promising one since its advantages regard bioactivity and osteogenic potential over conventional irregular shape ones [23]. Since the merits of spherical bioactive glass and considering the unique physical and chemical properties of RSNBGs, we hypothesize that the radial one possesses even higher than SNBGs whose superior bone conductivity and osteoinductivity have already been experimentally demonstrated. Build on this foundation, this study rigorously compares the effects of two different nano-bioactive glasses, namely SNBG and RSNBG on proliferation and osteogenic differentiation of rBMSCs in vitro, and discussed the feasibility and advantages of their application in clinical bone defect repair.

First, the surface of RSNBG produced larger and denser HCA than the SNBG after soaked in the SBF for 24 h, demonstrating therefore the higher biological activity of RSNBG over SNBG. Especially the SEM results showed that a small amount of sediment appeared on the surface of a few SNBG particles. In addition, no obvious new vibration bands were found when compared with the FTIR results of SNBG before and after mineralization. These results suggested that the mineralization degree of SNBG is

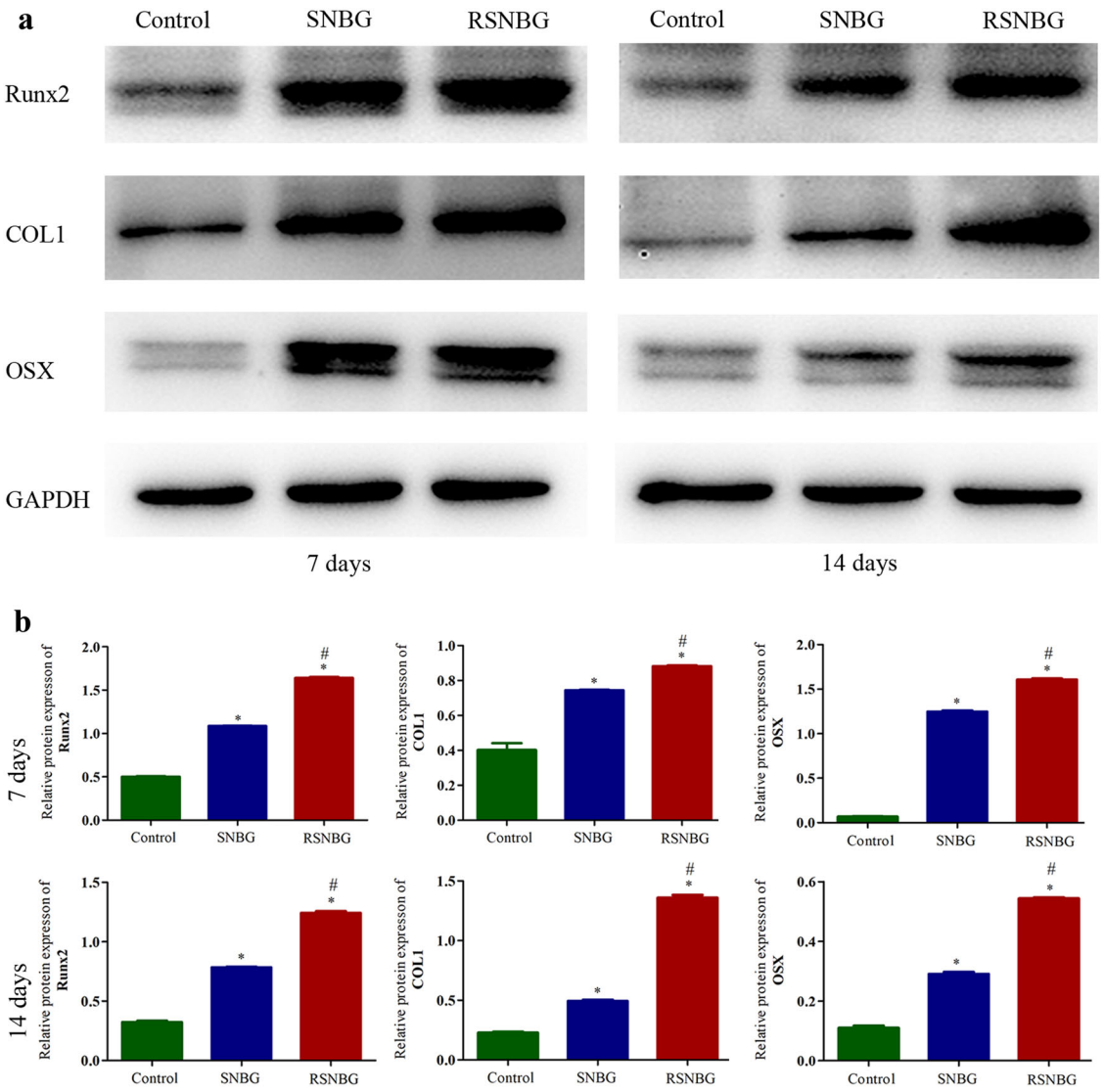

Fig. 8 Western blot analysis and densitometry analysis. Western blot analysis of the expression of relative proteins level (Runx2, COL1, and OSX) after 7 and 14 days of osteogenic-inducing culture (**a**). Densitometry analysis of each band was performed and calculated using GAPDH expression as a control (**b**). Control, not incubated with bioactive glass; SNBG, incubated with SNBG; RSNBG, incubated with RSNBG. ($n = 3$; $^{*}P < 0.05$, versus blank control group; $^{\#}P < 0.05$, RSNBG versus SNBG)

too weak, even if there is, to be detected through FTIR, so no new vibration band was shown in the FTIR spectrum.

Previous studies showed that proliferation and differentiation of osteoblasts are promoted by bioactive glass containing high concentrations of Si and Ca ions, a low concentration of P ions, and an appropriate CaO/SiO_2 ratio [32, 33]. In this study, the concentrations of Si and Ca ions were higher and the concentration of P ion was lower in the RSNBG extract compared with the SNBG extract. Our experimental data are in agreement with this finding, in which RSNBG showed higher efficiency on promoting cell proliferation and differentiation. However, the specific concentration and mechanism of these ions affecting cell proliferation and cell cycle remain to be elucidated [13].

Runx2, Col1, and Osx are osteogenesis-associated genes. Runx2, an essential transcription factor, regulates different stages of osteoblast differentiation and skeletal development [34]. Col1, produced by osteoblasts, is the main organic component of the bone matrix that later is being mineralized [35], and therefore is an important indicator of the osteogenic function of osteoblasts [36]. Osx is an early stage markers for osteoblast differentiation [37]. The current study revealed that rBMSCs incubated with RSNBG had significantly higher Runx2, Col1, and Osx mRNA levels and protein levels on days 7 and 14 compared with the rBMSCs incubated with SNBG and the control group ($P < 0.05$). Also, osteogenic gene expression and protein levels were also higher in rBMSCs incubated with 50 μg/mL SNBG

compared with the control group ($P < 0.05$). The results of RT-PCR and western blot further indicated that both SNBG and RSNBG can promote the differentiation of rBMSCs into osteoblasts and the mineralization of extracellular matrix.

Our experimental data also supports RSNBG had stronger osteogenic effects than SNBG through characterization of specific osteogenesis markers. In vitro, rBMSCs incubated with RSNBG exhibited higher ALP activity in early osteogenesis and produced more mineralized nodules in late osteogenesis ($P < 0.05$). We infer the better osteogenic effects compared with SNBG might be attributed to several unique properties of RSNBG. First, TEM results showed that RSNBG particles had fine branch-like structures with a radial channel surface, which increased the surface area and allowed faster ion release into the dissolution product and higher apatite forming bioactivity of RSNBG than SNBG [38, 39]. The large surface area of RSNBG can thereby provide an increased amount of protein binding sites on the surface of the material and results in enhanced protein adsorption [40]. Previous studies have shown that proteins adsorbed on the surface of materials promote the early interaction between materials and cells, providing the materials with higher bioactivity in the manner of activating the crosstalk between integrin expressed on cells and ligands attached on the surface of materials [36]. In the scenario of bone regeneration, this ligand that results higher osteogenic properties largely, or even exclusively, terms the HCA, a ligand that plays a key role in regulating osteogenesis. Increasing the absorption of which can provide an environment for adhesion and differentiation of bone progenitor cells, secretion of the bone matrix, and mineralization [1, 26]. After incubating in SBF, the HCA layer on the surface of SNBG was denser and more abundant than that of RSNBG.

5 Conclusion

In conclusion, SNBG and RSNBG both exhibit good biocompatibility due to the unique physicochemical properties, which significantly induced proliferation and osteogenic differentiation of rBMSCs. In particular, our data demonstrated, compared with SNBG, RSNBG is of higher efficiency in inducing osteogenic differentiation and mineralization in rBMSCs. Future studies should focus on the osteogenesis testing of SNBG and RSNBG in vivo to further evaluate its feasibility for clinical bone defect repair and reconstruction.

Acknowledgements This study was funded by grants from the National Key Research and Development Program of China (2016YFA0201704/2016YFA0201700), the Postdoctoral Science Foundation of Jiangsu Province (1701163B), the National Natural Science Foundation of China (81701025), and the Priority Academic Program Development of Jiangsu Higher Education Institutions (2014-37). All authors thank Xiaofeng Chen project group of the South China University of Technology for kindly providing bioactive glass.

Compliance with ethical standards

Conflict of interest The authors declare that they have no conflict of interest.

Publisher's note Springer Nature remains neutral with regard to jurisdictional claims in published maps and institutional affiliations.

References

1. Drago L, Toscano M, Bottagisio M. Recent evidence on bioactive glass antimicrobial and antibiofilm activity: a mini-review. Materials. 2018;11:326. https://doi.org/10.3390/ma11020326.
2. Buser Z, Brodke DS, Youssef JA, Meisel HJ, Myhre SL, Hashimoto R, et al. Synthetic bone graft versus autograft or allograft for spinal fusion: a systematic review. J Neurosurg Spine. 2016;25:509–16. https://doi.org/10.3171/2016.1.SPINE151005.
3. Ho-Shui-Ling A, Bolander J, Rustom LE, Johnson AW, Luyten FP, Picart C. Bone regeneration strategies: engineered scaffolds, bioactive molecules and stem cells current stage and future perspectives. Biomaterials. 2018;180:143–62. https://doi.org/10.1016/j.biomaterials.2018.07.017.
4. Iaquinta MR, Mazzoni E, Manfrini M, D'Agostino A, Trevisiol L, Nocini R, et al. Innovative biomaterials for bone regrowth. Int J Mol Sci. 2019;20:618. https://doi.org/10.3390/ijms20030618.
5. Bellucci D, Salvatori R, Anesi A, Chiarini L, Cannillo V. SBF assays, direct and indirect cell culture tests to evaluate the biological performance of bioglasses and bioglass-based composites: three paradigmatic cases. Mater Sci Eng C Mater Biol Appl. 2019;96:757–64. https://doi.org/10.1016/j.msec.2018.12.006.
6. Thomas A, Bera J. Preparation and characterization of gelatin-bioactive glass ceramic scaffolds for bone tissue engineering. J Biomater Sci Polym Ed. 2019;30:561–79. https://doi.org/10.1080/09205063.2019.1587697.
7. Granel H, Bossard C, Nucke L, Wauquier F, Rochefort GY, Guicheux J, et al. Optimized bioactive glass: the quest for the bony graft. Adv Healthc Mater. 2019;8:e1801542. https://doi.org/10.1002/adhm.201801542.
8. Hench LL, Splinter RJ, Allen WC, Greenlee TK. Bonding mechanisms at the interface of ceramic prosthetic materials. J Biomed Mater Res A. 1971;5:117–41. https://doi.org/10.1002/jbm.820050611.
9. Su TR, Chu YH, Yang HW, Huang YF, Ding SJ. Component effects of bioactive glass on corrosion resistance and in vitro biological properties of apatite-matrix coatings. Biomed Mater Eng. 2019;30:207–18. https://doi.org/10.3233/Bme-191045.
10. Ojansivu M, Wang X, Hyvari L, Kellomaki M, Hupa L, Vanhatupa S, et al. Bioactive glass induced osteogenic differentiation of human adipose stem cells is dependent on cell attachment mechanism and mitogen-activated protein kinases. Eur Cell Mater. 2018;35:54–72. https://doi.org/10.22203/eCM.v035a05.
11. Baino F, Novajra G, Miguez-Pacheco V, Boccaccini AR, Vitale-Brovarone C. Bioactive glasses: special applications outside the skeletal system. J Non Cryst Solids. 2016;432:15–30. https://doi.org/10.1016/j.jnoncrysol.2015.02.015.
12. Xynos ID, Edgar AJ, Buttery LDK, Hench LL, Polak JM. Gene-expression profiling of human osteoblasts following treatment with the ionic products of Bioglass 45S5 dissolution. J Biomed

Mater Res. 2001;55:151–7. https://doi.org/10.1002/1097-4636(200105)55:2<151::Aid-Jbm1001>3.3.Co;2-4.
13. Hoppe A, Guldal NS, Boccaccini AR. A review of the biological response to ionic dissolution products from bioactive glasses and glass-ceramics. Biomaterials. 2011;32:2757–74. https://doi.org/10.1016/j.biomaterials.2011.01.004.
14. Zhang D, Lepparanta O, Munukka E, Ylanen H, Viljanen MK, Eerola E, et al. Antibacterial effects and dissolution behavior of six bioactive glasses. J Biomed Mater Res A. 2010;93a:475–83. https://doi.org/10.1002/jbm.a.32564.
15. Ajita J, Saravanan S, Selvamurugan N. Effect of size of bioactive glass nanoparticles on mesenchymal stem cell proliferation for dental and orthopedic applications. J Biomed Mater Res A. 2015;53:142–9. https://doi.org/10.1016/j.msec.2015.04.041.
16. Srinivasan S, Jayasree R, Chennazhi KP, Nair SV, Jayakumar R. Biocompatible alginate/nano bioactive glass ceramic composite scaffolds for periodontal tissue regeneration. Carbohydr Polym. 2012;87:274–83. https://doi.org/10.1016/j.carbpol.2011.07.058.
17. Mačković M, Hoppe A, Detsch R, Mohn D, Stark WJ, Spiecker E, et al. Bioactive glass (type 45S5) nanoparticles: in vitro reactivity on nanoscale and biocompatibility. J Nanopart Res. 2012;14:966. https://doi.org/10.1007/s11051-012-0966-6.
18. Vichery C, Nedelec JM. Bioactive glass nanoparticles: from synthesis to materials design for biomedical applications. Materials. 2016;9:288. https://doi.org/10.3390/ma9040288.
19. Greenspan' DC, Zhong JP, Chen XF, LaTorre GP. The evaluation of degradability of melt and sol-gel derived Bioglass® in vitro. Bioceramics. 1997;10:391–4. https://doi.org/10.1016/B978-008042692-1/50093-5.
20. Suh WH, Suslick KS, Stucky GD, Suh YH. Nanotechnology, nanotoxicology, and neuroscience. Prog Neurobiol. 2009;87:133–70. https://doi.org/10.1016/j.pneurobio.2008.09.009.
21. Simchi A, Tamjid E, Pishbin F, Boccaccini AR. Recent progress in inorganic and composite coatings with bactericidal capability for orthopaedic applications. Nanomedicine. 2011;7:22–39. https://doi.org/10.1016/j.nano.2010.10.005.
22. Bush JR, Liang HX, Dickinson M, Botchwey EA. Xylan hemicellulose improves chitosan hydrogel for bone tissue regeneration. Polym Adv Technol. 2016;27:1050–5. https://doi.org/10.1002/pat.3767.
23. Wang SN, Gao XJ, Gong WY, Zhang ZC, Chen XF, Dong YM. Odontogenic differentiation and dentin formation of dental pulp cells under nanobioactive glass induction. Acta Biomater. 2014;10:2792–803. https://doi.org/10.1016/j.actbio.2014.02.013.
24. Wang YD, Liao TS, Shi M, Liu C, Chen XF. Facile synthesis and in vitro bioactivity of radial mesoporous bioactive glasses. Mater Lett. 2017;206:205–9. https://doi.org/10.1016/j.matlet.2017.07.021.
25. Li YL, Liang QM, Lin C, Li X, Chen XF, Hu Q. Facile synthesis and characterization of novel rapid-setting spherical sub-micron bioactive glasses cements and their biocompatibility in vitro. Mater Sci Eng C Mater Biol Appl. 2017;75:646–52. https://doi.org/10.1016/j.msec.2017.02.095.
26. Hench LL, Polak JM. Third-generation biomedical materials. Science. 2002;295:1014–7. https://doi.org/10.1126/science.1067404.
27. Salinas AJ, Martin AI, Vallet-Regi M. Bioactivity of three CaO-P2O5-SiO2 sol-gel glasses. J. Biomed Mater Res. 2002;61:524–32. https://doi.org/10.1002/jbm.10229.
28. Baino F, Hamzehlou S, Kargozar S. Bioactive glasses: where are we and where are we going. J Funct Biomater. 2018;9:25 https://doi.org/10.3390/jfb9010025.
29. Jones JR. New trends in bioactive scaffolds: the importance of nanostructure. J Eur Ceram Soc. 2009;29:1275–81. https://doi.org/10.1016/j.jeurceramsoc.2008.08.003.
30. Misra SK, Mohn D, Brunner TJ, Stark WJ, Philip SE, Roy I, et al. Comparison of nanoscale and microscale bioactive glass on the properties of P(3HB)/Bioglass composites. Biomaterials. 2008;29:1750–61. https://doi.org/10.1016/j.biomaterials.2007.12.040.
31. Karpov M, Laczka M, Leboy PS, Osyczka AM. Sol-gel bioactive glasses support both osteoblast and osteoclast formation from human bone marrow cells. J Biomed Mater Res A. 2008;84a:718–26. https://doi.org/10.1002/jbm.a.31386.
32. Lossdörfer S, Schwartz Z, Lohmann CH, Greenspan DC, Ranly DM, Boyan BD. Osteoblast response to bioactive glasses in vitro correlates with inorganic phosphate content. Biomaterials. 2004;25:2547–55. https://doi.org/10.1016/j.biomaterials.2003.09.094.
33. Meyer MB, Benkusky NA, Pike JW. The RUNX2 cistrome in osteoblasts: characterization, down-regulation following differentiation, and relationship to gene expression. J Biol Chem. 2014;289:16016–31. https://doi.org/10.1074/jbc.M114.552216.
34. Li CM, Vepari C, Jin HJ, Kim HJ, Kaplan DL. Electrospun silk-BMP-2 scaffolds for bone tissue engineering. Biomaterials. 2006;27:3115–24. https://doi.org/10.1016/j.biomaterials.2006.01.022.
35. Viguet-Carrin S, Garnero P, Delmas PD. The role of collagen in bone strength. Osteoporos Int. 2006;17:319–36. https://doi.org/10.1007/s00198-005-2035-9.
36. Wilson CJ, Clegg RE, Leavesley DI, Pearcy MJ. Mediation of biomaterial-cell interactions by adsorbed proteins: a review. Tissue Eng. 2005;11:1–18. https://doi.org/10.1089/ten.2005.11.1.
37. Ozeki M, Kuroda S, Kon K, Kasugai S. Differentiation of bone marrow stromal cells into osteoblasts in a self-assembling peptide hydrogel: in vitro and in vivo studies. J Biomater Appl. 2011;25:663–84. https://doi.org/10.1177/0885328209356328.
38. de Oliveira AAR, de Souza DA, Dias LLS, de Carvalho SM, Mansur HS, Pereira MD. Synthesis, characterization and cytocompatibility of spherical bioactive glass nanoparticles for potential hard tissue engineering applications. Biomed Mater. 2013;8:025011. https://doi.org/10.1088/1748-6041/8/2/025011.
39. Lei B, Chen XF, Wang YJ, Zhao NR, Du C, Fang LM. Surface nanoscale patterning of bioactive glass to support cellular growth and differentiation. J Biomed Mater Res A. 2010;94a:1091–9. https://doi.org/10.1002/jbm.a.32776.
40. Baier RE, Dutton RC. Initial events in interactions of blood with a foreign surface. J Biomed Mater Res. 1969;3:191–206. https://doi.org/10.1002/jbm.820030115.